Mean seasonal cycle of isothermal depth in the South China Sea

Tangdong Qu,[1] Yan Du,[1] Jianping Gan,[2] and Dongxiao Wang[3]

Received 13 March 2006; revised 15 September 2006; accepted 13 October 2006; published 20 February 2007.

[1] The mean seasonal cycle of isothermal depth is examined using all available temperature profiles in the South China Sea. On the annual average, the isothermal depth has two deep cores (>45 m). One extends westward from the Luzon Strait along the continental slope south of China, and the other in the deep basin of the southern South China Sea. Harmonic analysis shows that the seasonal variation of isothermal depth is predominantly annual in the northern South China Sea, exceeding 70 m in winter and falling below 20 m in summer near the continental slope south of China. The annual variation is weaker in the southern South China Sea, where the isothermal depth approaches its seasonal maximum (>55 m) in fall and minimum (<35 m) in spring. The semiannual variation is most prominent in the southern South China Sea, being of comparable strength with the annual variation. Among others, local Ekman pumping appears to be an important process responsible for the semiannual variation in the southern South China Sea. A detailed description of the month-to-month variations is provided, to set a basic background for further understanding the South China Sea mixed layer dynamics and thermodynamics.

Citation: Qu, T., Y. Du, J. Gan, and D. Wang (2007), Mean seasonal cycle of isothermal depth in the South China Sea, *J. Geophys. Res.*, *112*, C02020, doi:10.1029/2006JC003583.

1. Introduction

[2] The thickness of ocean's mixed layer or what is often termed the mixed layer depth (MLD) is an important factor influencing the sea surface temperature (SST). In the South China Sea, the largest marginal sea of the Southeast Asian waters, the MLD is modulated by the seasonal reversing monsoon, as well as the intrusion of the Kuroshio through the Luzon Strait [e.g., *Qu*, 2001; *Liu et al.*, 2004; *Gan et al.*, 2006]. In the mean time, the variation of MLD also feeds back to the atmosphere, especially during the development of summer monsoon [*Chu and Chang*, 1997; *Qu*, 2001]. On interannual timescales, the temporal correspondence between the South China Sea surface temperature and El Nino and Southern Oscillation (ENSO) has been reported [e.g., *Wang et al.*, 2000; *Xie et al.*, 2003; *Liu et al.*, 2004; *Qu et al.*, 2004; *Wang et al.*, 2006]. Through the interaction between an anomalous atmospheric circulation and the underlying mixed layer dynamics, the impact of ENSO can be conveyed from the Pacific into the South China Sea. This explains why the warm SST anomaly in the South China Sea peaks in the ensuing summer of El Nino, up to six months after the atmospheric anomalies reach their maximum strength. The South China Sea MLD is therefore important to study, for both its regional and global significance in climate variability.

[3] The South China Sea MLD has been studied in the past decades. Most of the earlier studies, however, used synoptic observations collected from hydrographic cruises, and the phenomena described might be true only for some particular locations and seasons. Given the fact that the South China Sea MLD, as in many other parts of the global ocean, is variable on a range of spatial and temporal scales, results from synoptic observations may not be representative of the mean fields. To the best of our knowledge, the only climatological interpretations of the South China Sea MLD were prepared by *Qu* [2001] and *Du* [2002]. The former focused on the mixed layer dynamics associated with the southwest monsoon onset and did not provide an entire seasonal cycle of MLD. The latter was based on the gridded temperature and salinity from World Ocean Atlas 1998 (WOA98). Since the objective analysis used in preparing the WOA98 involved heavy smoothing along pressure surfaces, changes in vertical gradient around the depth of pycnocline may not be especially realistic, and as a consequence, *Du* [2002] failed to show many detailed structures of the South China Sea MLD.

[4] It seems more appropriate to produce the MLD from each individual density profile than from a heavily smoothed climatology (e.g., WOA98). Such a study is not available primarily due to the lack of sufficient density profiles in the South China Sea. Considering that the number of temperature profiles is larger by about an order than that of density profiles [*Qu*, 2001], the present study is intended to provide a comprehensive description of the mean seasonal cycle of isothermal depth (ID), a good proxy

[1]International Pacific Research Center, SOEST, University of Hawaii at Manoa, Honolulu, Hawaii, USA.
[2]Department of Mathematics and Atmospheric, Marine and Coastal Environment Program, Hong Kong University of Science and Technology, Kowloon, Hong Kong, China.
[3]Key Laboratory of Tropical Marine Environmental Dynamics, South China Sea Institute of Oceanology, Chinese Academy of Sciences, Guangzhou, China.

Copyright 2007 by the American Geophysical Union.
0148-0227/07/2006JC003583

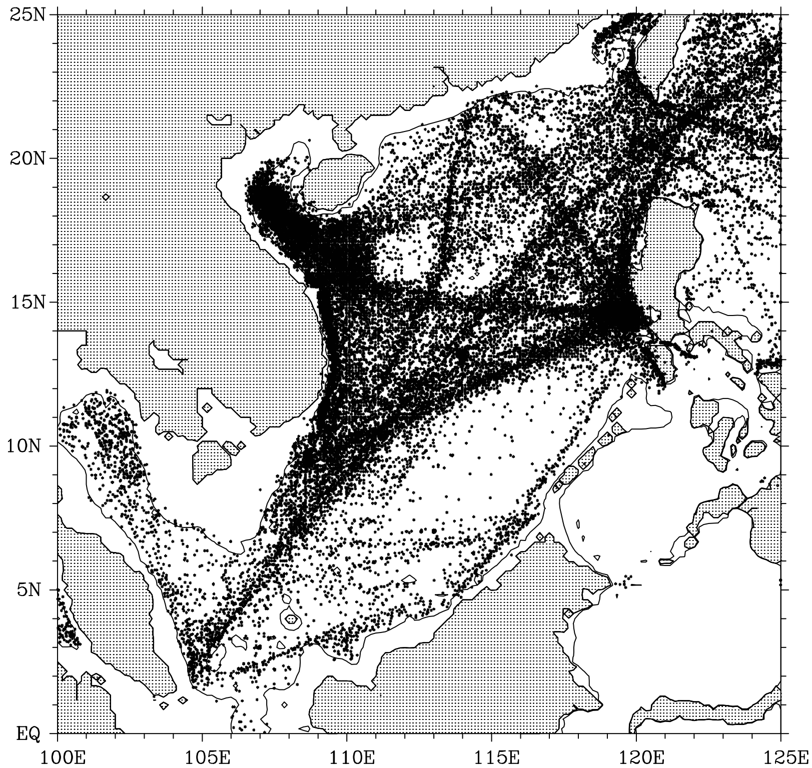

Figure 1. Geographical distribution (asterisks) of temperature profiles used for this study, which consist of 39,429 profiles extending to 50 m or below.

of MLD, using all available temperature profiles in the South China Sea. Climatological surface wind and heat flux data are also analyzed to explore the processes that possibly affect the ID seasonal variation. Results of the analysis are presented in the following sections. After a brief description of the data and methods of analysis in section 2, we will describe the general characteristics of the South China Sea ID in section 3. The correspondence of ID with atmospheric forcing is examined in section 4, and the month-to-month variations are discussed in section 5. Results are summarized in section 6, and an error analysis is provided in Appendix A.

2. Data and Methods of Analysis

[5] For this study temperature data at observed levels archived in the World Ocean Database 2001 (WOD01) from the region between 0° and 25°N and between 100° and 125°E were used (Figure 1). We first selected the data by dropping those profiles that were flagged as "bad" or as not passing the monthly, seasonal, and annual standard deviation checks. We then removed those profiles that did not extend to 50 m, thus instantaneously eliminating profiles over the shallow continental shelf, and those profiles with obviously erroneous records (e.g., temperature <10°C) and exceptionally sparse vertical separation (>20 m) between two samples in the upper 100 m. Different vertical separation criteria (10 m, 30 m, 50 m, etc.) can also be chosen, provided the question of sensitivity is born in mind, but the results remain qualitatively unchanged (see Appendix A). The final data set provided a total of 39,429 temperature profiles in the South China Sea (Figure 1). In time, the data spanned the period from the 1920s to the beginning of the new century; no obvious bias in the density of sampling was apparent toward any season of the year. In space, the upper ocean was best sampled in the northern and central South China Sea, while the data coverage in the southeastern part of the basin was relatively poor.

[6] The definition of ID was based on a variable temperature criterion. We computed the ID from individual temperature profiles as where water temperature is 0.8°C cooler than a near-surface value at 10 m. Note that the temperature increment selected is well consistent with the optimal estimate suggested by *Kara et al.* [2000], and in a qualitative sense, the South China Sea ID is insensitive to the selection of this temperature increment. The IDs estimated from individual profiles were then averaged in $0.5° \times 0.5°$ boxes for each month regardless the year of observations. To eliminate the bias in the density of sampling, a variable scan-radius was chosen so that each average was based on at least 10 samples. Standard deviations were also calculated and used to edit the mean field of ID (see Appendix A). If an estimate from an individual profile deviated from the grid mean by a value three times larger than the standard deviation, it was excluded and the mean and standard deviation were recalculated. The gridded ID fields were finally smoothed using a two-dimensional Gaussian filter, with e-folding scales of 1° in longitude and latitude and 1 month in time.

[7] To explore the generating mechanisms linked to the ID seasonal variation, we have also included a climatology of surface heat flux [*Oberhuber*, 1988] based on the Comprehensive Ocean and Atmosphere Data Set (COADS) and a climatology of wind stress based on the European

21562202c, 2007, C2, Downloaded from https://agupubs.onlinelibrary.wiley.com/doi/10.1029/2006JC003583 by Hong Kong University Of, Wiley Online Library on [18/08/2026]. See the Terms and Conditions (https://onlinelibrary.wiley.com/terms-and-conditions) on Wiley Online Library for rules of use; OA articles are governed by the applicable Creative Commons License

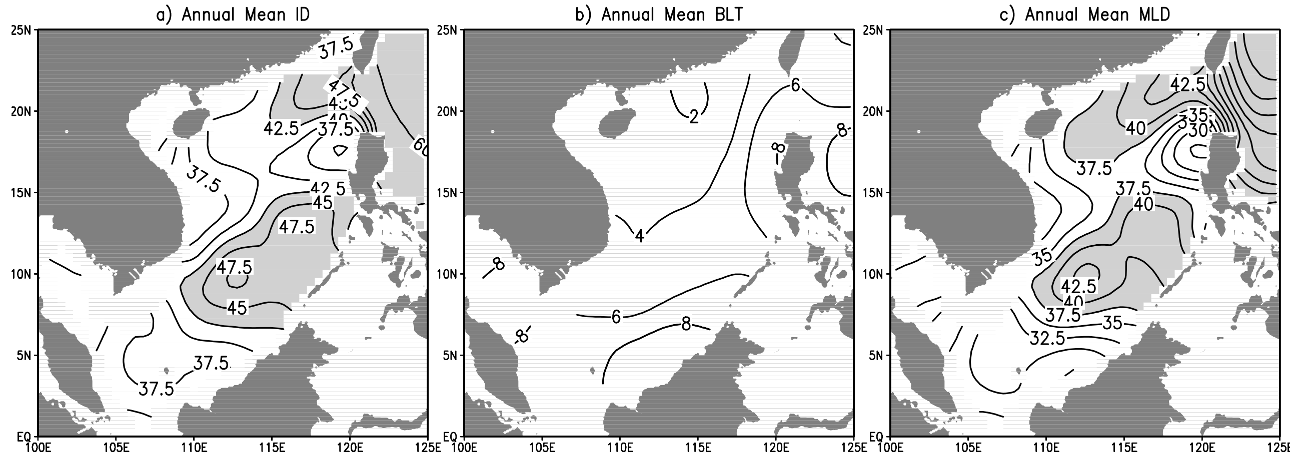

Figure 2. Annual mean (a) isothermal depth (ID), (b) barrier layer thickness (BLT), and (c) mixed layer depth (MLD) in meters.

Remote Sensing (ERS) satellite microwave scatterometer measurements. Both climatologies had reasonable resolutions in the South China Sea. The ERS wind data originally consisted of two parts: ERS1 spanning from August 1991 to May 1996, and ERS2 panning from April 1996 to January 2001. They were averaged to construct a monthly climatology of wind stress.

3. General Description

3.1. Annual Mean Distribution

[8] The annual mean ID was produced from monthly mean values to reduce bias stemming from seasonally uneven sampling. Over a large part of the South China Sea, the annual mean ID is deeper than 40 m (Figure 2a), and shows essentially the same pattern as described by *Qu* [2001] using a critical temperature gradient criterion of 0.05°C m^{-1}. Coinciding with the West Luzon Eddy and East Vietnam Eddy [*Shaw et al.*, 1999; *Qu*, 2000], we see two shallow ID cores (<35 m), which divide the deep basin of the South China Sea roughly into two parts. In the north, there is a deep ID tongue (>45 m) extending southwestward from the Luzon Strait along the continental slope south of China. This deep ID tongue corresponds well with the prevailing northeasterly wind, downward Ekman pumping, and surface cooling (Figure 3), indicative of strong influence of the northeast winter monsoon. Another potentially important influence is due to the intrusion of the Kuroshio, which supplies well-mixed western Pacific surface water to the South China Sea. In the south, the annual mean ID is deeper than 45 m, with a core extending roughly from 110°E, 8°N to 120°, 15°N. The southwest summer monsoon seems to be primarily responsible for the deep ID in the southern South China Sea. The detail will be discussed in section 4.

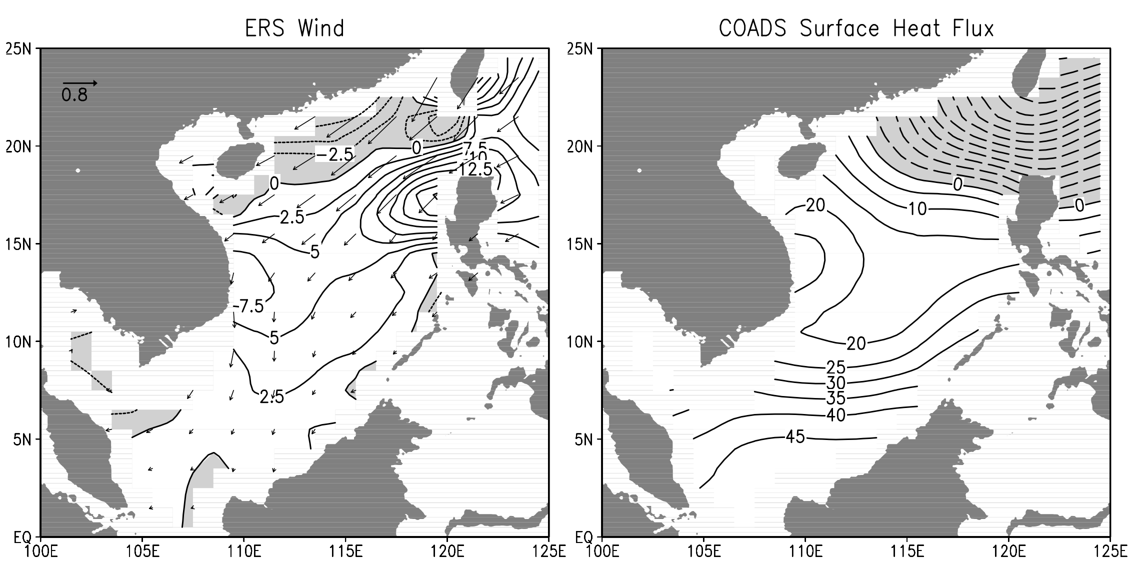

Figure 3. Annual mean (a) ERS wind stress vectors (10^{-1} Pa), wind stress curl (10^{-8} Pa m^{-1}), and (b) COADS surface heat flux (W m^{-2}).

21562202c, 2007, C2, Downloaded from https://agupubs.onlinelibrary.wiley.com/doi/10.1029/2006JC003583 by Hong Kong University Of, Wiley Online Library on [18/08/2026]. See the Terms and Conditions (https://onlinelibrary.wiley.com/terms-and-conditions) on Wiley Online Library for rules of use; OA articles are governed by the applicable Creative Commons License

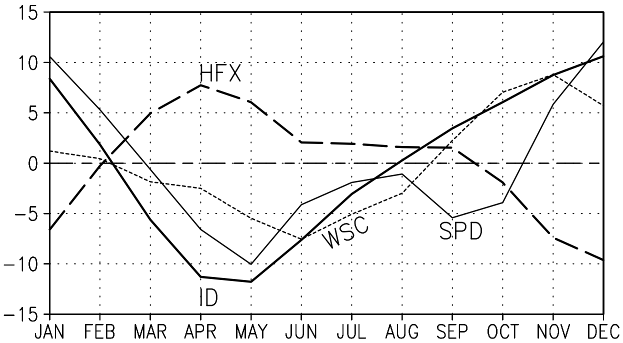

Figure 4. Seasonal variation of isothermal depth (ID; heavy solid line), COADS surface heat flux (HFX; heavy dashed line), ERS wind speed (SPD; light solid line), and ERS wind stress curl (WSC; light doted line) averaged over the entire South China Sea. Units are m for ID, 10 W m^{-2} for HFX, 0.25 m s^{-1} for SPD, and 5×10^{-9} Pa m^{-1} for WSC. Annual mean values of 41 m, 2×10 W m^{-2}, 4.3 m s^{-1}, and 19×10^{-9} Pa m^{-1} have been removed before plotting.

[9] Examination of all (2,280) available density profiles that passed the monthly, seasonal, and annual standard deviation checks and had a vertical resolution better than 20 m in the upper 100 m shows that the MLD is generally shallower than the ID by 2–8 m on the annual average (Figure 2b), implying the presence of a barrier layer [*Lukas and Lindstrom*, 1991] in the South China Sea. Here the MLD is determined as where potential density, σ_θ, is equal to the sea surface σ_θ plus the increment in σ_θ equivalent to a net decrease of 0.8°C in temperature. The barrier layer is relatively thick in the southern South China Sea, and can reach as much as 8 m along the Philippine and Borneo coast, presumably as a result of large excess of precipitation over evaporation there [*Wu et al.*, 2001; *Du et al.*, 2004]. With the limitation of existing density profiles, we are unable to show the barrier layer thickness seasonal variation. On the annual average, the spatial distribution of ID (Figure 2a) resembles that of MLD (Figure 2c) in almost all the details. To take advantage of the larger number of temperature profiles in the South China Sea, we focus our following analysis on the ID, which we believe is an important step toward a complete understanding of the MLD seasonal variation. The full implication of barrier layer thickness seasonal variation requires further investigation.

3.2. Basin-Wide Variation

[10] The South China Sea ID is governed, among others, by the large-scale atmospheric circulation and sea surface heat flux [*Wang et al.*, 2000; *Xie et al.*, 2003; *Liu et al.*, 2004]. To better describe this basin-wide response, we simply average the ID over the entire South China Sea basin (denoted as $\overline{ID}$ hereinafter). The annual mean $\overline{ID}$ in the South China Sea is 41 m, shallower than that on the Pacific side of the Luzon Strait by 10–20 m (Figure 2a). The shallower $\overline{ID}$ in the South China Sea is presumably a result of upward Ekman pumping (Figure 3a). Since the South China Sea is a semiclosed basin at depths below about 200 m, cold water must upwell from the subsurface in order to establish a stable thermocline which otherwise would be gradually diminished by the downward surface heat flux (Figure 3b).

[11] The $\overline{ID}$ in the South China Sea has a maximum in December and a minimum in May (Figure 4). This seasonal variation has an extremely good correspondence with surface heat flux (r = −0.93) and wind speed (r = 0.78), suggesting that the large-scale atmospheric processes are primarily responsible for the basin-wide variation in the South China Sea. The Ekman pumping affects the $\overline{ID}$ in an opposite phase to the $\overline{ID}$ seasonal variation. But, on the basin wide, its effect is well suppressed by the large-scale atmospheric circulation and surface heat flux.

3.3. Annual and Semiannual Harmonics

[12] Annual and semiannual harmonic analyses are conducted to provide an overview of the ID seasonal variation in the South China Sea. As one would expect, the largest annual variation occurs near the continental slope south of China, where its maximum amplitude exceeds 24 m (Figure 5a), reflecting strong influence of monsoonal winds, as well as the intrusion of the Kuroshio [*Gan et al.*, 2006]. The annual variation is relatively weak elsewhere, falling below 8 m in the deep basin southeast of Vietnam. In a large part of the northwestern basin, the ID reaches its seasonal maximum in January, corresponding well with the prevailing northeast monsoon. This signal is led by 1–3 months in the rest of the basin. The semiannual variation is weaker, in general, by a factor about 2 (Figure 5b). Its amplitude has two cores (>8 m). One is located at the northwestern corner of the basin, and the other lies in the south, centered at about (111°E, 8°N). The northern core reaches its maximum strength in January and July, about one month earlier than the southern one.

[13] To better document the relative importance of annual and semiannual variations, the seasonal variation of ID is presented along 111°E (Figure 6), and it reveals a large phase difference between regions to the south and north of about 12°N. The maximum ID in the south occurs around August–September, leading that in the north by 3–4 months. Similar difference is seen in the phase when the ID is minimum. At about 8°N, the semiannual variation is most pronounced and of comparable strength with the annual variation. As we progress northward along the section, the annual variation becomes dominant. At about 18°N, the amplitude of annual variation is about three times larger than that of semiannual variation. In summer, the annual and semiannual variations tend to be out of phase, and their large degree of cancellation results in a nearly constant ID from April through September.

[14] The semiannual signal gets weaker as we progress to the east (Figure 5). At 115°E, the seasonal variation of ID is predominantly annual and has a northward phase propagation, with the phase near the southern end of the section leading that near the northern end of the section by about two months (Figure 7). This provides some independent evidence for the northeastward propagation of the onset of summer monsoon in the South China Sea and the western Pacific as well [e.g., *Wu and Wang*, 2001]. In the south, the ID is shallowest in April/May, in correspondence with the spring warm pool [*Chu and Chang*, 1997; *Qu*, 2001]. The ID deepens as the summer monsoon starts to prevail and approaches its seasonal maximum in October/November.

21562202c, 2007, C2, Downloaded from https://agupubs.onlinelibrary.wiley.com/doi/10.1029/2006JC003583 by Hong Kong University Of, Wiley Online Library on [18/08/2026]. See the Terms and Conditions (https://onlinelibrary.wiley.com/terms-and-conditions) on Wiley Online Library for rules of use; OA articles are governed by the applicable Creative Commons License

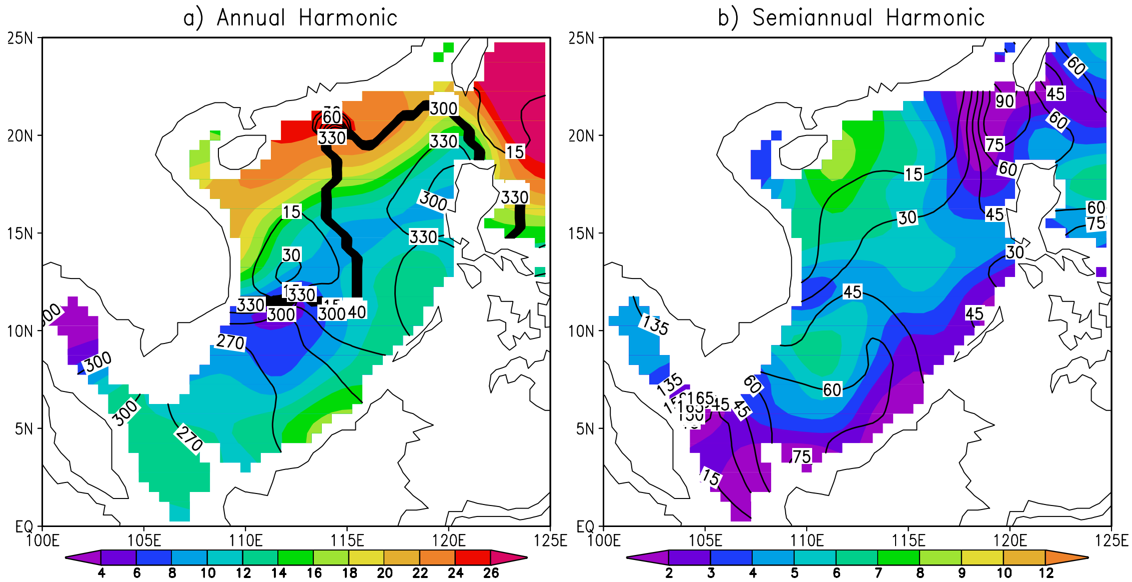

Figure 5. Amplitude (color) of (a) annual and (b) semiannual harmonics of isothermal depth (m). The phase (contours) corresponds to the day of the year when mixed layer depth is maximum.

In the north, the ID has a seasonal minimum in June–July and a seasonal maximum in December–January.

4. Correspondence With Atmospheric Forcing

[15] The ocean's mixed layer dynamics has been widely studied in literature [e.g., *Davis et al.*, 1981; *Bleck et al.*, 1989; *Murtugudde et al.*, 1995; *Thompson et al.*, 2002]. According to these earlier studies, the deepening (shoaling) of mixed layer, representing a downward (upward) buoyancy flux, is determined by a number of processes. Among others, wind stirring, surface cooling, and Ekman pumping are of particular importance. Wind stirring is the primary energy source to maintain the turbulent entrainment across the bottom of the mixed layer. Surface cooling provides necessary buoyancy flux to maintain the surface convection, which is particularly important at ocean's middle and high latitudes. Ekman pumping, more oriented with local topography and coastline, affects the mixed layer mainly through upwelling.

[16] To gain an overview of how the South China Sea ID is related to the atmospheric forcing described above, a multiple cross-correlation analysis was conducted (Figure 8). In the region roughly north of 10°N, the ID has high correlations with both wind speed and surface heat flux, indicative of the dominant influence of wind stirring and surface cooling. Negative correlation is seen between ID and wind stress curl in the northwestern corner of the basin, implying that the

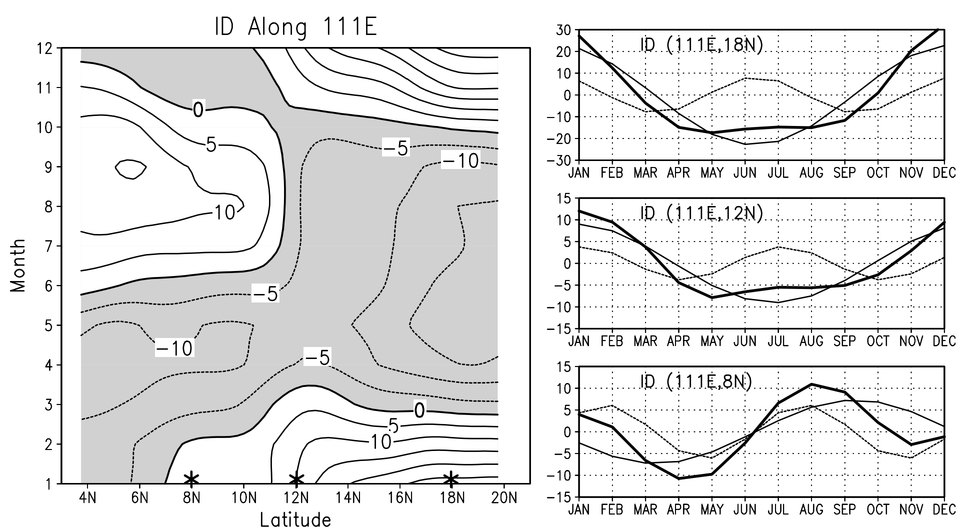

Figure 6. (left) Seasonal variation of isothermal depth along 111°E. Areas with negative values are shaded. (right) Seasonal variation of isothermal depth (heavy solid) and its annual (light solid) and semiannual (light dotted) components at (111°E, 8°N), (111°E, 12°N), and (111°E, 18°N). The locations are shown on the left panel. The annual mean values have been subtracted before plotting.

21562202c, 2007, C2, Downloaded from https://agupubs.onlinelibrary.wiley.com/doi/10.1029/2006JC003583 by Hong Kong University Of, Wiley Online Library on [18/08/2026]. See the Terms and Conditions (https://onlinelibrary.wiley.com/terms-and-conditions) on Wiley Online Library for rules of use; OA articles are governed by the applicable Creative Commons License

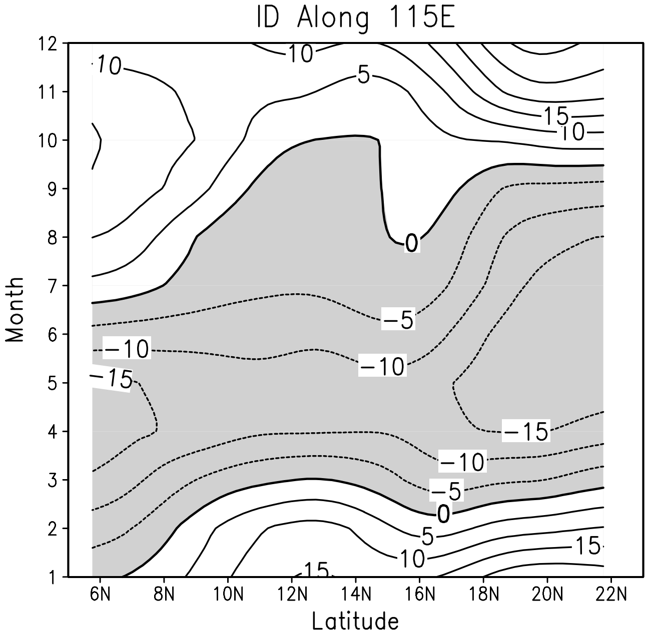

Figure 7. Same as the left panel of Figure 6 except along 115°E.

piling up (drawing off) of surface water forced by the monsoonal wind also plays a role in the ID seasonal variation. The correlation is positive near the west coast of the Philippines, suggesting weaker influence of Ekman pumping on the ID seasonal variation over the region. Wind stirring and surface cooling become less important as we progress southward. In the southern South China Sea, mostly to the south of 10°N, the correlations of ID with both wind speed and surface heat flux fall below 0.5 (Figures 8a and 8c). Only the correlation with wind stress curl satisfies the 95% confidence level criterion in a small region around (110°E, 6°N). We will return to this point later.

[17] Harmonic analyses of wind speed, wind stress curl, and surface heat flux were also conducted to further identify the relative importance of these processes in determining the ID seasonal variation. Along the continental slope south of China, the annual amplitudes of all the three processes are large, though their geographic locations are slightly different (Figure 9), corresponding well with the large annual variation of ID (Figure 5). The annual amplitudes of wind speed and surface heat flux drop rapidly toward the south, by a factor at least 5 in the region south of about 10°N. In contrast, the annual amplitude of wind stress curl has a local maximum (>16 × 10^{-8} Pa m^{-1}) around 8°N. There, the downward Ekman pumping peaks during the southwest monsoon (Figure 9), and as a consequence, the ID deepens toward its seasonal maximum in September–October (Figure 5), around the end of the season when Ekman pumping is negative. Apparently, this seasonal maximum of ID cannot be accounted for by the annual variation of wind stirring and surface cooling which lag the ID by 2–4 months (Figure 9). Further inspection of wind speed shows a second maximum in July, in correspondence with the prevailing southwest summer monsoon. The enhanced wind stirring and downward Ekman pumping at this season lead to a maximum ID in September–October and on the annual average, explains the deep ID core in the southern South China Sea (Figure 2a).

[18] The amplitudes of semiannual variations in wind speed and surface heat flux show similar patterns. Both have a maximum off the southeastern tip of Vietnam at 10°–12°N (Figure 9), corresponding to the maximum strength of monsoon in January and July, respectively. The semiannual variation in wind speed and surface heat flux is weak elsewhere. The semiannual variations in ID (Figure 5b) coincide well with wind stress curl (Figure 9). In the north, along the continental slope south of China, the semiannual amplitude of wind stress curl exceeds 8 × 10^{-8} Pa m^{-1}, and the upward Ekman pumping depletes surface water out of the region, resulting in minimum ID in March and September, respectively (Figures 5 and 6). In the south, mostly to the south of 10°N, the wind stress curl has maxima in May and November (Figure 9), leading the ID minima by about a month (Figures 5 and 6). The semiannual signal is related to the onset of southwest summer monsoon, which disrupts the warming of the southern South China Sea and leads to a shoaling of ID, as well as a cooling of SST in summer [*Xie et al.*, 2003]. It is worthwhile to note

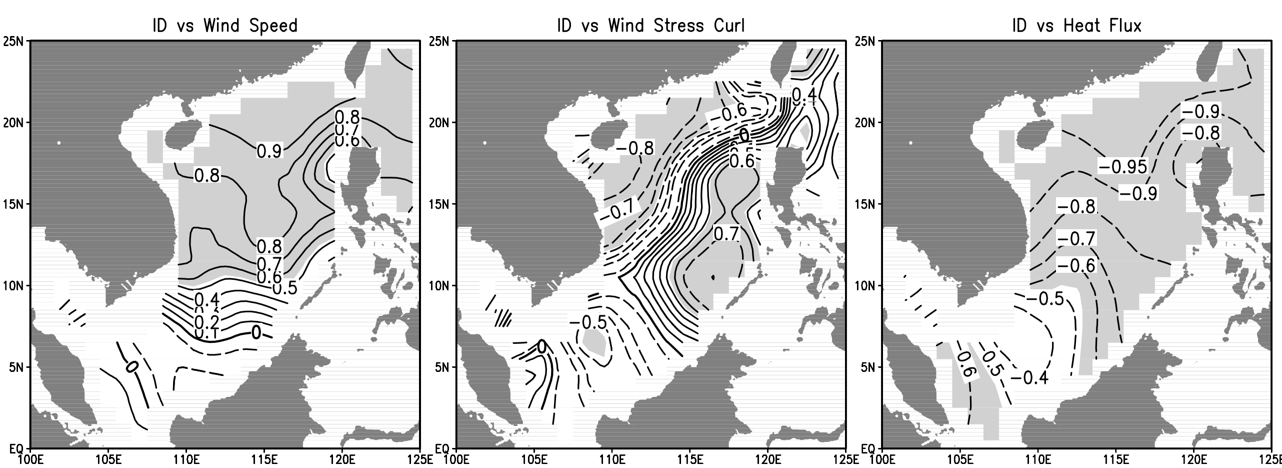

Figure 8. Correlation between the isothermal depth and ERS wind speed (left), ERS wind stress curl (middle), and COADS surface heat flux (right). Contour interval is 0.1, and areas where the 95% confidence level criterion (t-test) is satisfied are shaded.

21562202c, 2007, C2, Downloaded from https://agupubs.onlinelibrary.wiley.com/doi/10.1029/2006JC003583 by Hong Kong University Of, Wiley Online Library on [18/08/2026]. See the Terms and Conditions (https://onlinelibrary.wiley.com/terms-and-conditions) on Wiley Online Library for rules of use; OA articles are governed by the applicable Creative Commons License

21562202c, 2007, C2, Downloaded from https://agupubs.onlinelibrary.wiley.com/doi/10.1029/2006JC003583 by Hong Kong University Of, Wiley Online Library on [18/08/2026]. See the Terms and Conditions (https://onlinelibrary.wiley.com/terms-and-conditions) on Wiley Online Library for rules of use; OA articles are governed by the applicable Creative Commons License

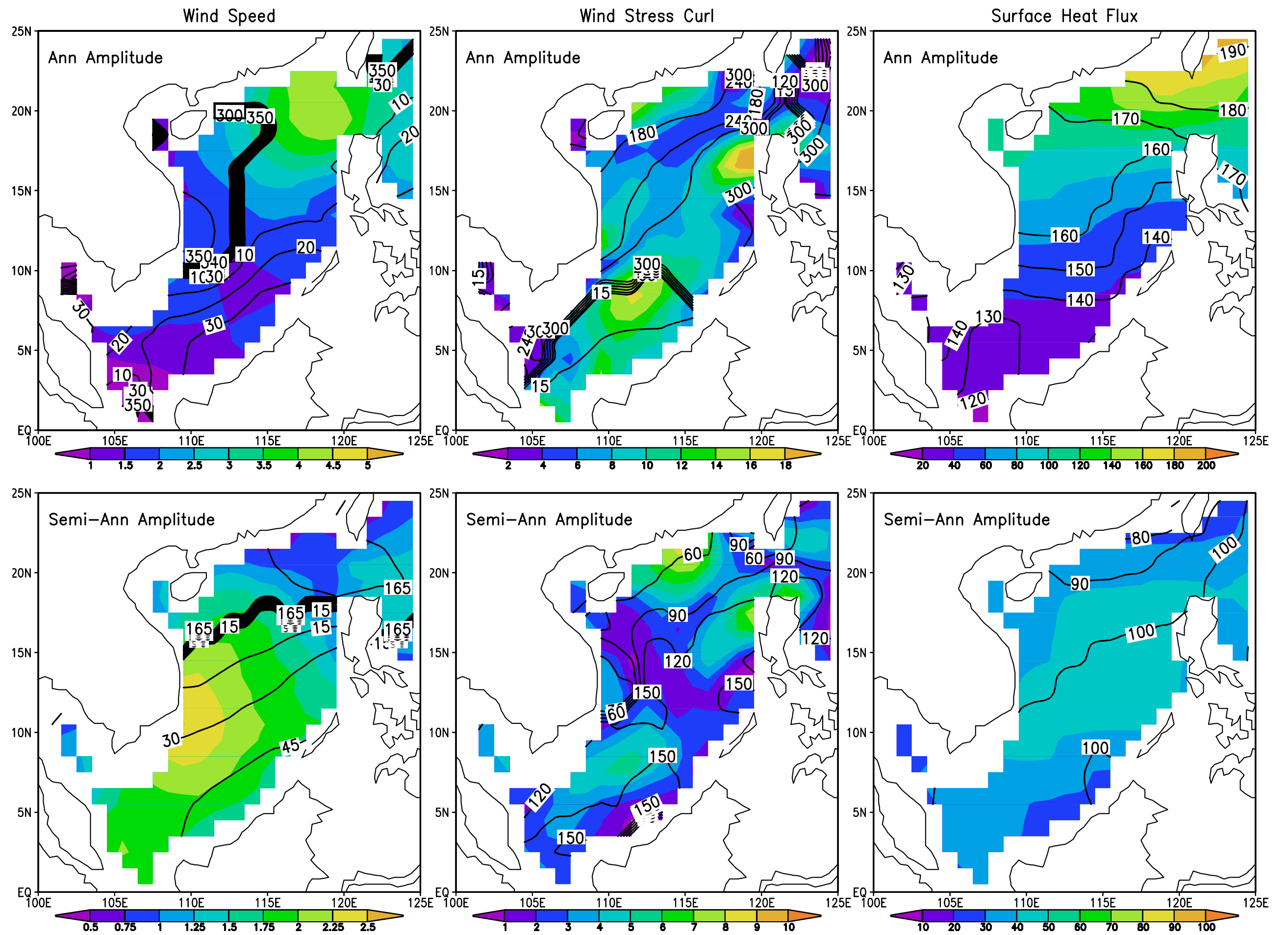

Figure 9. Same as Figure 5 except for ERS wind speed in m s^{-1} (left), ERS wind stress curl in 10^{-8} Pa m^{-1} (middle), and COADS surface heat flux in W m^{-2} (right).

that the wind stress curl also shows a maximum semiannual variation near the northern tip of Luzon. But, no such a signal is seen in the ID (Figure 5b). The implication of this result is that large-scale atmospheric circulation and surface heat flux are dominant in determining the ID seasonal variation over the region.

[19] Also important to note is that there is an apparent southward phase propagation in wind stress curl (Figure 9). On the annual timescale, the maximum wind stress curl first occurs near the continental slope south of China in June/July and about six months later in the southern South China Sea. The phase difference for semiannual variation is about three months. Careful examination of the ID variation shows a weak northward rather than southward propagation on the annual timescale, but mostly confined in the southern South China Sea (Figure 5a). This pattern is well consistent with the annual variation of surface heat flux (Figure 9). On the semiannual timescale, the southward phase propagation in the ID (Figure 5b) can only be explained by the wind stress curl, giving additional evidence for its importance in regulating the ID semiannual variation.

5. Month-to-Month Variations

[20] This section provides a detailed description of the ID month-to-month variations (Figure 10). In January, when the northeast monsoon fully develops, wind stirring, downward Ekman pumping (Figure 11), and surface cooling (Figure 12) work together generating a seasonal maximum of ID (>70 m) near the continental slope south of China. *Wang et al.* [2001] noted that because of the deep thermocline at this season, incorporating with enhanced western boundary current, ventilation of the thermocline occurs in the northern South China Sea, a phenomenon that only appears in the mid-latitudes of the Ocean. The ID decreases toward the south, falling below 40 m in the southeastern corner of the basin. As the northeast monsoon diminishes, wind stress cannot provide enough turbulent kinetic energy to maintain the deep ID created in winter, and as a result, the ID shoals over the entire basin of the South China Sea. In March, the ID remains deeper than 50 m only in a small region off southwest Taiwan, and is dominated by a bowl-shaped distribution elsewhere, deeper (>45 m) in the central part of the basin and shallower (<35 m) near the boundary. This distribution is consistent with earlier observations of sea level [*Shaw et al.*, 1999], suggesting an anticyclonic circulation in the upper ocean during this period of the year [*Wu et al.*, 1998].

[21] The ID continues to shoal (Figure 10), as surface heat flux turns positive (Figure 12) and wind stress reaches its seasonal minimum (Figure 11) during the transition season of monsoon. The ID falls below 35 m in most parts

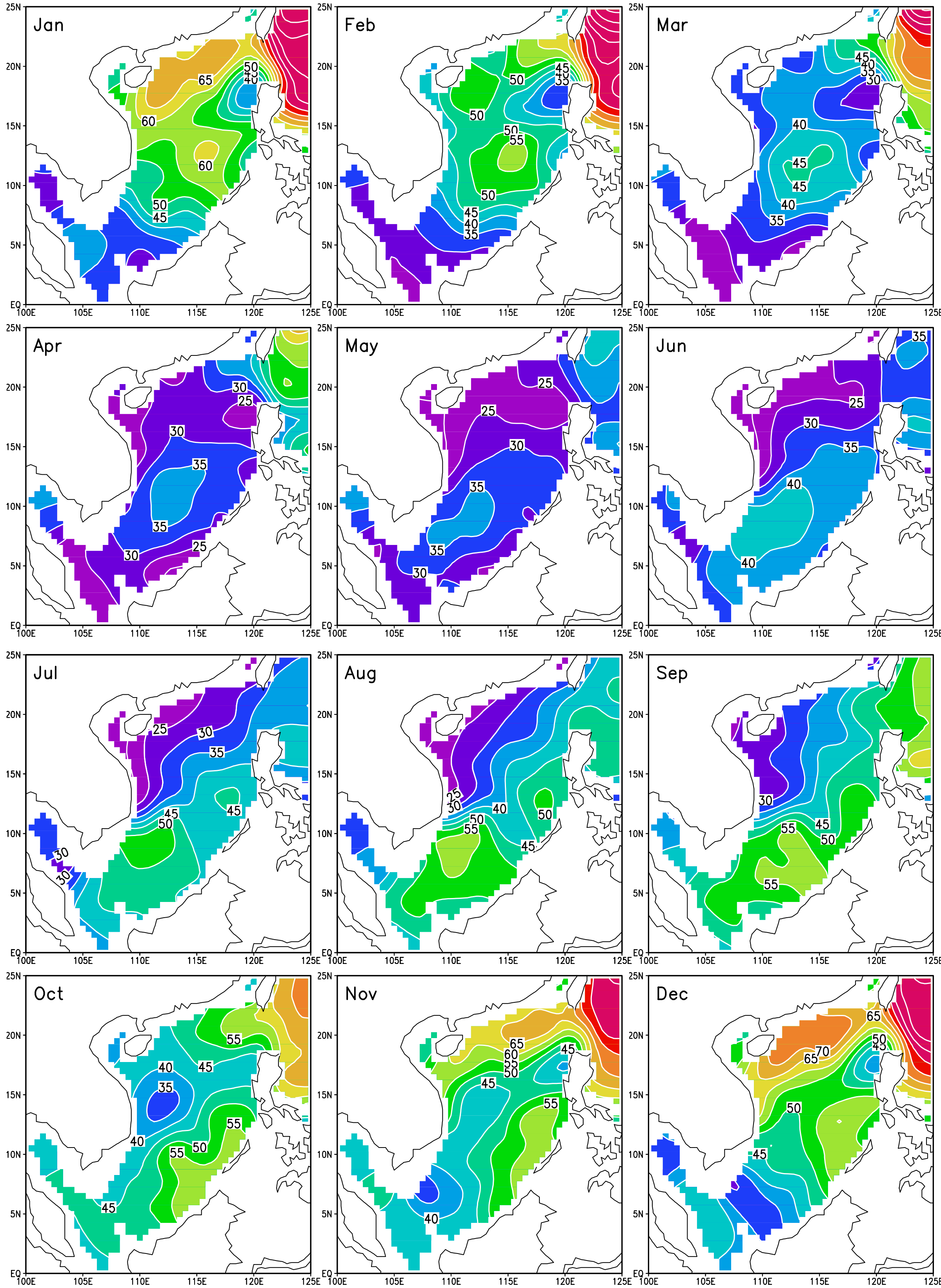

Figure 10. Month-to-month variations of isothermal depth (m).

21562202c, 2007, C2, Downloaded from https://agupubs.onlinelibrary.wiley.com/doi/10.1029/2006JC003583 by Hong Kong University Of, Wiley Online Library on [18/08/2026]. See the Terms and Conditions (https://onlinelibrary.wiley.com/terms-and-conditions) on Wiley Online Library for rules of use; OA articles are governed by the applicable Creative Commons License

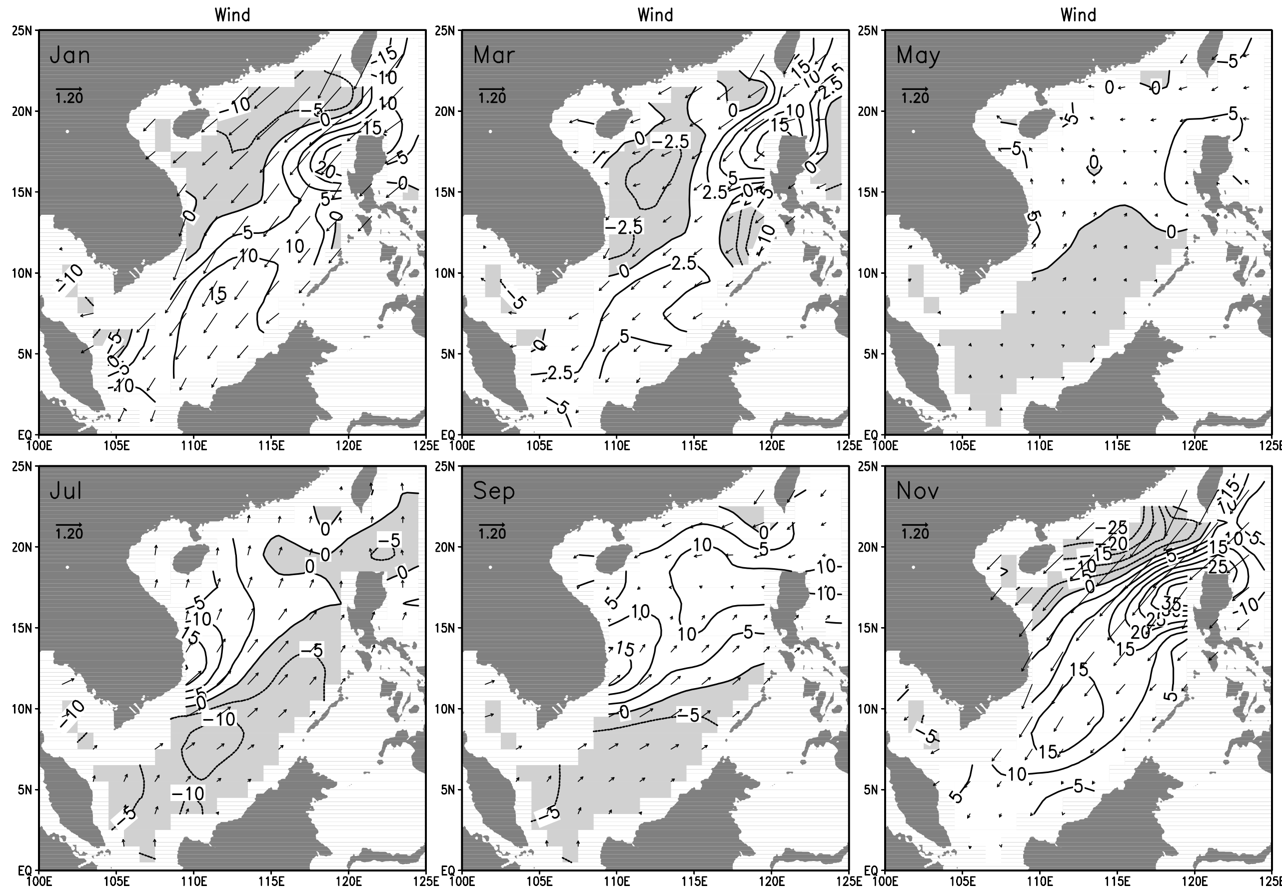

Figure 11. ERS wind stress vectors (10^{-1} Pa) and wind stress curl (10^{-8} Pa m^{-1}) in January, March, May, July, September, and November. Contour interval is 5×10^{-8} Pa m^{-1}, with two additional contours of 2.5×10^{-8} and -2.5×10^{-8} Pa m^{-1} for March and May.

of the basin in April. The bowl-shaped distribution shifts slightly southward, reflecting the fact that the ID has different rates of variation at different latitudes (Figures 6 and 7). The ID reaches its seasonal minimum in May, and as a direct consequence, heat gained from the atmosphere is well trapped in the surface layer. This induces a warm SST in a large part of the southern South China Sea [*Qu*, 2001], often referred to as the spring warm pool [*Chu and Chang*, 1997], and provides a necessary condition for the onset of summer monsoon.

[22] As summer monsoon develops, the mixed layer starts to deepen in the south. In June, the maximum ID exceeds 40 m off the southeast tip of Vietnam (Figure 10). This ID maximum corresponds well with a negative wind stress curl (Figure 11). *Xie et al.* [2003] noted that, as the southwest monsoon wind impinges on the north–south running maintain range on the east coast of Vietnam, a strong wind jet occurs at its southeastern tip, resulting in a cold filament that spreads northeastward offshore. To the south of the cold filament, an anticyclonic circulation develops (Figure 11), generating a local ID maximum (Figure 10). The ID continues to deepen in July (>50 m), and reaches its seasonal maximum (>55 m) in August–September, around the end of the season when wind stress curl is negative.

[23] The wind stress curl in summer is mostly positive in the northern South China Sea, with the zero line extending northeastward roughly from the southeastern tip of Vietnam to the northwestern tip of Luzon (Figure 11). The maximum wind stress curl (>20×10^{-8} Pa m^{-1}) occurs off east Vietnam, immediately to the north of the cold filament described by *Xie et al.* [2003]. In response, we see a shallow ID over a large part of the northern South China Sea. The distribution of ID is essentially oriented in the southeast–northwest direction (Figure 10), consistent with those of wind stress curl (Figure 11) and surface heat flux (Figure 12). The minimum ID falls below 25 m in the northwestern corner of the basin, while the core of positive wind stress curl is located somewhat farther southward. In addition to surface heating that helps generate a stronger surface stratification near the northern boundary, wind stirring is another possible process that shifts the minimum ID away from the southeast coast of Vietnam. As noted by *Xie et al.* [2003], the cold filament observed offshore of the southeastern tip of Vietnam occurs consistently around the wind speed maximum. The strong wind stirring may cause entrainment of more colder and denser water into the mixed layer from below, thus resulting in a deeper ID in the region immediately to the north of the cold filament where maximum wind stress curl is observed (Figure 10).

[24] In contrast with what shown in the northwestern corner of the basin, the ID is relatively deep near the west coast of Luzon, reaching >50 m in late summer (Figure 10).

21562202c, 2007, C2, Downloaded from https://agupubs.onlinelibrary.wiley.com/doi/10.1029/2006JC003583 by Hong Kong University Of, Wiley Online Library on [18/08/2026]. See the Terms and Conditions (https://onlinelibrary.wiley.com/terms-and-conditions) on Wiley Online Library for rules of use; OA articles are governed by the applicable Creative Commons License

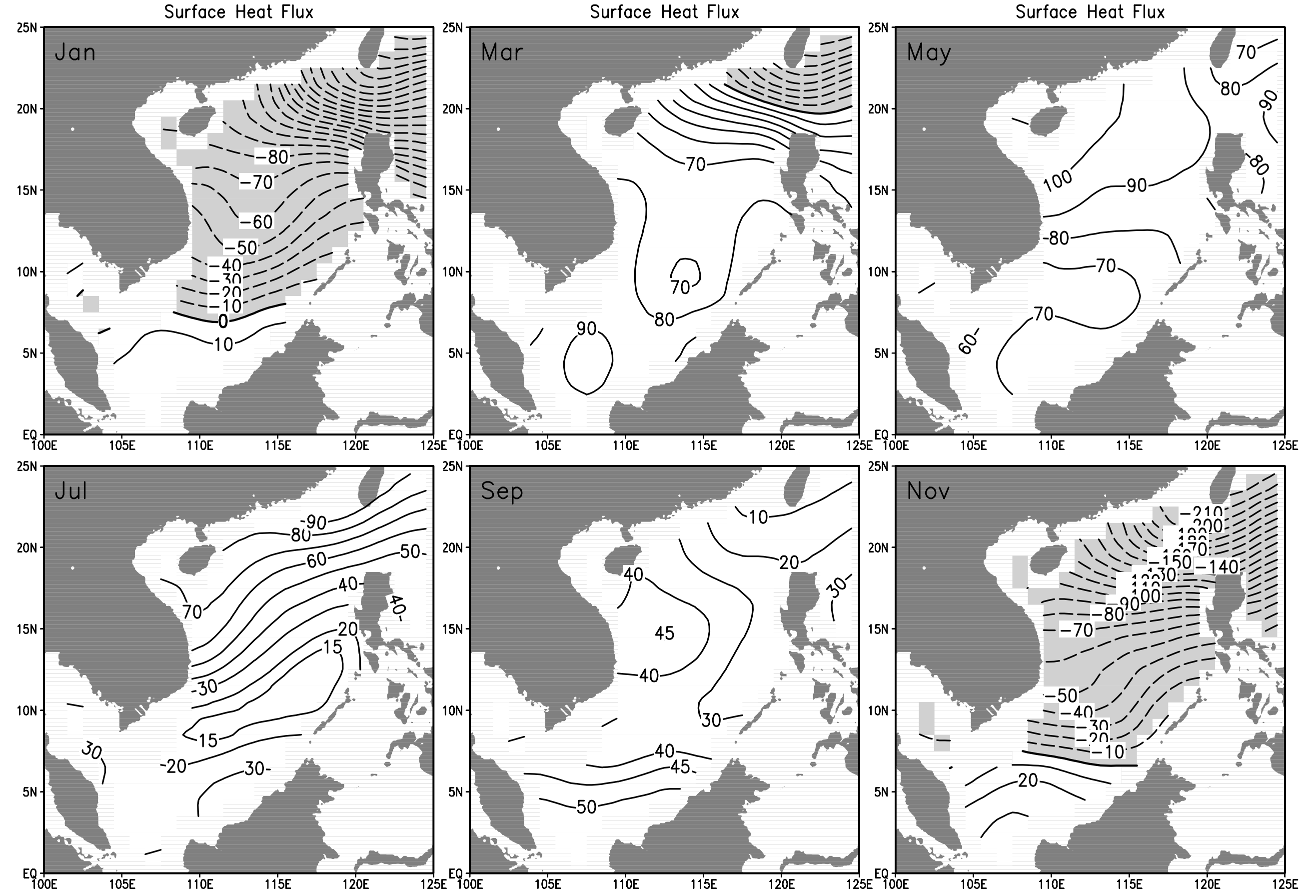

Figure 12. Same as Figure 11 except for COADS surface heat flux in W m^{-2}. Contour interval is 10 W m^{-2}.

The deep ID seems to be connected with the Philippine Seas, consistent with earlier studies on the Pacific influence through the Luzon Strait [e.g., *Hu et al.*, 2000; *Qu et al.*, 2000; *Gan et al.*, 2006]. An implication of this result is that the intrusion of the Kuroshio through the Luzon Strait may play a role influencing the South China Sea ID. The deep ID near the west coast of Luzon could also be due to local recirculation, supplying relatively well-mixed surface water from the south [e.g., *Fang et al.*, 1998]. The present data, unfortunately, do not allow for a further investigation. We leave this for future numerical studies.

[25] The northeast monsoon starts to prevail in September/October (Figure 11), and this results in the deepening of ID near the continental slope south of China (Figure 10). In October, shallow ID (<35 m) remains only in a small region off east Vietnam, and a core of deep ID (>50 m) is seen extending westward from the Luzon Strait, an additional evidence for the influence of Pacific variability [*Shaw*, 1991; *Qu et al.*, 2000]. As the northeast monsoon fully develops in December, the ID is deeper than 45 m in the northern South China Sea, mostly to the north of 10°N, and reaches as deep as 70 m near the continental slope south of China. Interestingly, with the prevailing northeast monsoon, the ID does not get deeper everywhere as one would expect. Instead, it shoals in two small areas. One is around the southwestern corner of the deep basin, and the other is off the west coast of Luzon. The former is likely induced by the reflection of western boundary current near the Sunda Shelf, while the latter could be a result of upward Ekman pumping (Figure 11).

[26] We note that, although the seasonal variation of ID cannot be accounted for by Ekman pumping near the west coast of Luzon (Figure 8), the two have a good correspondence in space (Figures 10 and 11). Coinciding with the West Luzon Eddy, a local minimum of ID is present from October through April, nearly in phase with a local maximum in Ekman pumping. The upward Ekman pumping forced by the northeast monsoon lifts the base of the mixed layer and produces a shallower ID. This forms a contrast with its surroundings where Ekman pumping is relatively weak. The spatial distribution of ID is well consistent with the surface dynamic height distribution from hydrographic data [*Qu*, 2000], as well as the sea level distribution from satellite altimeter data [*Shaw et al.*, 1999].

6. Summary

[27] This study provides a detailed description of isothermal depth, a good proxy of MLD, and its seasonal variation in the South China Sea. On the annual average, the ID in the deep basin of the South China Sea has two cores (>45 m). One extends westward from Luzon Strait along the continental slope south of China, and the other in the south, extending from about 110°E, 8°N to 120°, 15°N. Both cores reflect strong influence of monsoon. The northern core seems to be dominated by the wind stirring and cooling convection associated with the northeast winter monsoon, while the southern one is more related to the wind stirring and downward Ekman pumping forced by the southwest summer monsoon.

21562202c, 2007, C2, Downloaded from https://agupubs.onlinelibrary.wiley.com/doi/10.1029/2006JC003583 by Hong Kong University Of, Wiley Online Library on [18/08/2026]. See the Terms and Conditions (https://onlinelibrary.wiley.com/terms-and-conditions) on Wiley Online Library for rules of use; OA articles are governed by the applicable Creative Commons License

[28] A basin-wide variation of ID is examined to better understand the influence of large-scale atmospheric circulation and surface heat flux. Averaged over the entire South China Sea, the seasonal variation of ID is dominated by the annual signal, with a maximum in December and a minimum in May. Wind stirring and surface cooling are primarily responsible for the basin-wide variation.

[29] The seasonal variation of ID is predominantly annual in the northern South China Sea, where the ID is deeper than 70 m in winter and shallower than 20 m in summer. Wind stirring and cooling convection seem to be dominant in the annual variation along the continental slope south of China. Here we emphasize that the effect of Ekman pumping is not negligible. This is particularly true in summer, when both wind stirring and cooling convection become weak. The annual variation of ID gets weaker in the southern South China Sea, approaching its seasonal maximum in fall and minimum in spring.

[30] The semiannual variation of ID is of comparable strength with the annual variation in the southern South China Sea, mostly to the south of 10°N. There, the ID reaches its seasonal maxima in February and August and seasonal minima in May and November. We attribute a large part of this semiannual variation to the local Ekman pumping forced by the southwest summer monsoon, in addition to the enhanced wind stirring. The semiannual variation also has a core near the northwestern corner of the basin, but its amplitude is smaller by a factor about three than the annual variation.

[31] With the existing climatological data, we are able to show that the mean seasonal cycle of ID in the South China Sea is due a large part to wind stirring, Ekman pumping, and cooling convection. A potentially important process overlooked in our analysis is the horizontal advection by ocean circulation of both local and remote origins. The influence of the Kuroshio intrusion through the Luzon Strait is apparent along the continental slope south of China coast and east of Vietnam. Modeling studies will be needed to further investigate the influence of horizontal advection and in particular, the role of local verses remote forcing in regulating the ID seasonal variation. We believe that a good understanding of ID seasonal variation and its forcing mechanisms in the South China Sea will provide important insight into the role of mixed layer dynamics in climate variability of the region.

Appendix A: Error Analysis

[32] The uncertainty in the mean ID was measured by standard deviation also obtained during average (section 2). Then, divided by the square root of the numbers of observations (≥10), the standard deviation was converted to the standard error. The standard error in the monthly mean ID is primarily due to interannual and mesoscale variability, in addition to the bad quality of some early observations. In general, the standard error is higher in winter and lower in summer. Averaged over the year, the standard error in the monthly mean ID ranges from about 3 to 5 m (Figure A1). The highest standard error (~5 m) occurs near the continental slope south of China, reflecting strong influence of Pacific variability through the Luzon Strait. Over a large part of the South China Sea, roughly to

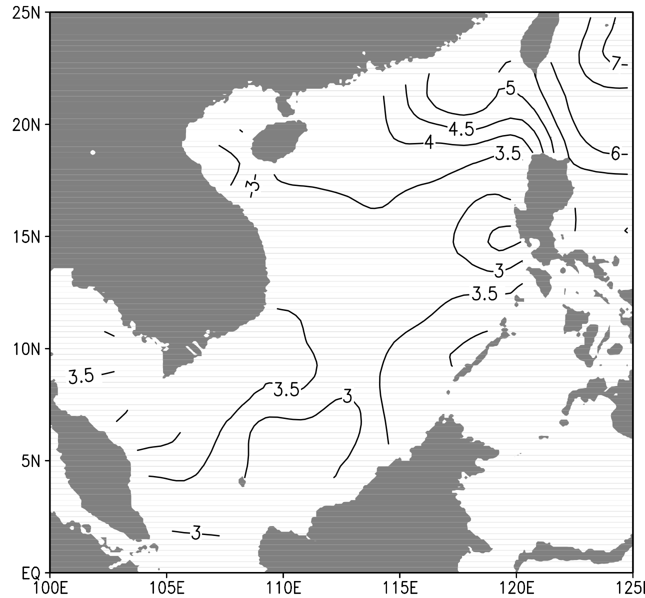

Figure A1. Annually averaged standard error in the monthly mean isothermal depth (m), based on ≥10 observations in each grid bin.

the south of about 18°N, the standard error in the monthly mean ID is 3–4 m. The standard error in the long-term annual mean ID is less than 2 m. With the contour intervals of 2.5 and 5 m selected in displaying the long-term annual (Figure 2) and monthly mean (Figure 10) ID, the large-scale phenomena presented in this study are mostly robust.

[33] Another source of uncertainty in the mean ID may be due to poor vertical resolution of the data. We first screened the data using a vertical resolution of 50 m and removed those profiles with a vertical separation larger than 50 m between two samplings in the upper 100 m. Then, we increased the vertical resolution to 30, 20, and 10 m to better resolve the ID from each individual temperature profile. Although the total number of observations decreases, from 80,157 to 63,098, 39,429, and 30,113, respectively, the mean ID only shows some minor differences, and the basic structure remains nearly unchanged. This result seems to suggest that the uncertainty in the mean ID due to poor vertical resolution of individual profiles can be significantly reduced by the combined use of more than 10 samples collected in various cruises in different years.

[34] **Acknowledgments.** This research was supported by the National Aeronautics and Space Administration through grant NAG5-12756. Support was also from Japan Agency for Marine-Earth Science and Technology through its sponsorship of the International Pacific Research Center (IPRC), from Research Grant Council of Hong Kong through grant CERG601204, and from NSF of China through grants 40406006, 40576013, and 40640420557. The authors are grateful to all the four anonymous reviewers for their thoughtful comments and constructive suggestions. Although not all their concerns can be addressed in the present paper, they provide important directions for our future studies. IPRC contribution number IPRC-416 and School of Ocean and Earth Science and Technology contribution number 7010.

References

Bleck, R., H. Hanson, D. Hu, and E. B. Kraus (1989), Mixed layer-thermocline interaction in a three-dimensional isopycnic coordinate model, *J. Phys. Oceanogr.*, *19*, 1417–1439.

21562202c, 2007, C2, Downloaded from https://agupubs.onlinelibrary.wiley.com/doi/10.1029/2006JC003583 by Hong Kong University Of, Wiley Online Library on [18/08/2026]. See the Terms and Conditions (https://onlinelibrary.wiley.com/terms-and-conditions) on Wiley Online Library for rules of use; OA articles are governed by the applicable Creative Commons License

Chu, P. C., and C. P. Chang (1997), South China Sea warm pool in boreal spring, *Adv. Atmos. Sci.*, *14*, 195–206.
Davis, R. E., R. deSzoeke, and P. P. Niiler (1981), Variability in the upper ocean during MILE. Part II: Modeling the mixed layer response, *Deep Sea Res., Part A*, *28*, 1453–1475.
Du, Y. (2002), Seasonal dynamics of the mixed layer and thermocline in the South China Sea, Ph.D. dissertation, 240 pp., Ocean Univ. of China, Qingdao.
Du, Y., D. Wang, P. Shi, P. Guo, and J. Chen (2004), Seasonal variation of the barrier layer in the South China Sea and its relationship to the sea surface flux, *Chin. J. Atmos. Sci.*, *28*, 101–111.
Fang, G., W. Fang, Y. Fang, and K. Wang (1998), A survey of studies on the South China Sea upper ocean circulation, *Acta Oceanogr. Taiwan*, *37*, 1–16.
Gan, J., H. Li, E. N. Curchitser, and D. B. Haidvogel (2006), Modeling South China Sea circulation: Response to seasonal forcing regimes, *J. Geophys. Res.*, *111*, C06034, doi:10.1029/2005JC003298.
Hu, J., H. Kawamura, H. Hong, and Y. Qi (2000), A review on the currents in the South China Sea: seasonal circulation, South China Sea warm current, and Kuroshio intrusion, *J. Oceanogr.*, *56*, 607–624.
Kara, A. B., P. A. Rochford, and H. E. Hurlburt (2000), An optimal definition for ocean mixed layer depth, *J. Geophys. Res.*, *105*, 16,803–16,821.
Liu, Q., X. Jiang, S.-P. Xie, and W. T. Liu (2004), A gap in the Indo-Pacific warm pool over the South China Sea in boreal winter: Seasonal development and interannual variability, *J. Geophys. Res.*, *109*, C07012, doi:10.1029/2003JC002179.
Lukas, R., and E. Lindstrom (1991), The mixed layer of the western equatorial Pacific Ocean, *J. Geophys. Res.*, *96*, 3343–3357.
Murtugudde, R., M. Cane, and V. Prasad (1995), A reduced-gravity, primitive Equation, isopycnal ocean GCM: Formulation and simulations, *Mon. Weather Rev.*, *123*, 2864–2887.
Oberhuber, J. M. (1988), An atlas based on the "COADS" data set: The budgets of heat, buoyancy and turbulent kinetic energy at the surface of the global ocean, *Rep. 15*, Max Planck Inst. für Meteorol., Hamburg, Germany.
Qu, T. (2000), Upper layer circulation in the South China Sea, *J. Phys. Oceanogr.*, *30*, 1450–1460.
Qu, T. (2001), Role of ocean dynamics in determining the mean seasonal cycle of the South China Sea surface temperature, *J. Geophys. Res.*, *106*, 6943–6955.
Qu, T., H. Mitsudera, and T. Yamagata (2000), Intrusion of the North Pacific waters into the South China Sea, *J. Geophys. Res.*, *105*, 6415–6424.
Qu, T., Y. Y. Kim, M. Yaremchuk, T. Tozuka, A. Ishida, and T. Yamagata (2004), Can Luzon Strait Transport play a role in conveying the impact of ENSO to the South China Sea?, *J. Clim.*, *17*, 3644–3657.
Shaw, P.-T. (1991), Seasonal variation of the intrusion of the Philippine sea water into the South China Sea, *J. Geophys. Res.*, *96*, 821–827.
Shaw, P.-T., S.-Y. Chao, and L.-L. Fu (1999), Sea surface height variations in the South China Sea from satellite altimetry, *Oceanol. Acta*, *22*, 1–17.
Thompson, L., K. Kelly, A. Darr, and R. Hallberg (2002), Buoyancy and mixed layer effects on the sea surface height response in an isopycnal model of the North Pacific, *J. Phys. Oceanogr.*, *32*, 3657–3670.
Wang, B., R. Wu, and X. Fu (2000), Pacific-East Asian teleconnection: How does ENSO affect East Asian climate?, *J. Clim.*, *13*, 1517–1536.
Wang, C., W. Q. Wang, D. X. Wang, and Q. Wang (2006), Interannual variability of the South China Sea associated with El Niño, *J. Geophys. Res.*, *111*, C03023, doi:10.1029/2005JC003333.
Wang, D., Y. Du, and P. Shi (2001), Evidence for thermocline ventilation in the South China Sea in winter, *Chin. Sci. Bull.*, *46*, 774–778.
Wu, C.-R., P.-T. Shaw, and S.-Y. Chao (1998), Seasonal and interannual variation of the velocity field of the South China Sea, *J. Oceanogr.*, *54*, 361–372.
Wu, R., and B. Wang (2001), Multi-stage onset of the summer monsoon over the western North Pacific, *Clim. Dyn.*, *17*, 277–289.
Wu, W., M. Tomczak, X. Fang, and D. Wu (2001), The barrier layer in the southern region of the South China Sea, *Chin. Sci. Bull.*, *46*(16), 1388–1392.
Xie, S.-P., Q. Xie, D. Wang, and W. T. Liu (2003), Summer upwelling in the South China Sea and its role in regional climate variations, *J. Geophys. Res.*, *108*(C8), 3261, doi:10.1029/2003JC001867.

Y. Du and T. Qu, International Pacific Research Center, SOEST, University of Hawaii at Manoa, 1680 East-West Road, Honolulu, HI 96822, USA. (tangdong@hawaii.edu)

J. Gan, Department of Mathematics and Atmospheric, Marine and Coastal Environment Program, Hong Kong University of Science and Technology, Kowloon, Hong Kong, China.

D. Wang, Key Laboratory of Tropical Marine Environmental Dynamics, South China Sea Institute of Oceanology, Chinese Academy of Sciences, 510301 Guangzhou, China.

21562202c, 2007, C2, Downloaded from https://agupubs.onlinelibrary.wiley.com/doi/10.1029/2006JC003583 by Hong Kong University Of, Wiley Online Library on [18/08/2026]. See the Terms and Conditions (https://onlinelibrary.wiley.com/terms-and-conditions) on Wiley Online Library for rules of use; OA articles are governed by the applicable Creative Commons License